Journal of Marine Systems 226 (2022) 103652

Contents lists available at ScienceDirect

Journal of Marine Systems

journal homepage: www.elsevier.com/locate/jmarsys

A *Lagrangian approach* to the Atlantic Jet entering the Mediterranean Sea: Physical and biogeochemical characterization

Iria Sala [a,b,*], Marina Bolado-Penagos [c,**], Ana Bartual [a], Miguel Bruno [c], Carlos M. García [a], Ángel López-Urrutia [d], Cristina González-García [e,f], Fidel Echevarría [a]

[a] Departamento de Biología, Facultad de Ciencias del Mar y Ambientales, Instituto Universitario de Investigaciones Marinas (INMAR), Campus de Excelencia Internacional del Mar (CEI-MAR), Universidad de Cádiz, Puerto Real, 11510 Cádiz, Spain
[b] Department of Mathematics and Statistics, University of Strathclyde, G1 1XH Glasgow, United Kingdom
[c] Departamento de Física Aplicada, Facultad de Ciencias del Mar y Ambientales, Instituto Universitario de Investigaciones Marinas (INMAR), Campus de Excelencia Internacional del Mar (CEI-MAR), Universidad de Cádiz, 11510 Puerto Real, Cádiz, Spain
[d] Instituto Español de Oceanografía (IEO), Centro Oceanográfico de Gijón, 33212 Gijón, Asturias, Spain
[e] Departamento de Ecología y Gestión Costera, Instituto de Ciencias Marinas de Andalucía (ICMAN-CSIC), Puerto Real, 11510 Cádiz, Spain
[f] Departamento de Ecología y Biología Animal, Universidad de Vigo, 36210 Vigo, Spain

ARTICLE INFO

Keywords:
Submesoscale processes
Chlorophyll patchiness
Phytoplankton
Lagrangian experiment
Strait of Gibraltar
Atlantic Jet

ABSTRACT

The temporal evolution of the physical and biogeochemical properties of the Atlantic Jet (AJ) along the first ~ 75 m of the water column during a 4-day journey was analysed by following the trajectory of a drifter dragged by the jet from the Strait of Gibraltar towards the Alborán Sea. Three stages were differentiated based on the evolution of several variables (e.g., velocity, temperature, nutrients, fluorescence). (i) Within the Strait of Gibraltar, the water column was primarily influenced by the tidal cycle, leading to a nutrient-enrichment of surface waters. However, due to the short residence time, the phytoplankton community that was mainly dominated by diatoms, did not demonstrate significant changes. (ii) Once outside the Strait, the drifter trajectory was mainly influenced by the frontal dynamics associated with the AJ. The drifter moved forward along the jet but also laterally across it and was continuously attracted to the mainstream (maximum current speed) or detached to its southern edge (minimum current speed). Due to the associated upwelling processes induced by the intensification of the current along the mainstream, the water column was characterized by colder, nutrient-richer water and lower fluorescence values. Conversely, along the southern edge of the jet, the water column was characterized by higher temperature, low nutrient concentration, and higher fluorescence. Along the first stations of this stage, diatom total abundance and biovolume continuously increased, reaching values ~ 12-times higher than the initial concentrations. (iii) In the last stage, the water parcel was still influenced by the frontal dynamics but with less intensity. Additionally, the colder and denser water of the AJ and the associated phytoplankton community subducted progressively as it moved into the region surrounded by warmer waters. Concomitantly, fluorescence and diatoms total abundance and biovolume decreased and were influenced by the decline of nutrient availability and the increase of mesozooplankton. Our results reveal the coupled processes induced by the entrance of the AJ in the Alborán Sea and highlight the strong control of the physical environment over the ecological processes in this region.

1. Introduction

The Strait of Gibraltar is the narrow exchange passage connecting the Alborán Sea, the westernmost basin of the Mediterranean Sea, and the Gulf of Cádiz which opens to the north Atlantic Ocean. Water exchange is usually described as a typical two-layer inverse-estuarine circulation that is induced by the negative hydrological budget of the Mediterranean Sea (e.g., Armi and Farmer, 1988). This circulation pattern leads to a natural tendency for oligotrophy in the Mediterranean basin that is associated with the surface flow towards the Alborán Sea of the relatively fresh and nutrient-poor Atlantic water (i.e., the Atlantic Jet) and a deep outflow of salty and nutrient-rich Mediterranean water towards the Atlantic Ocean (e.g., Armi and Farmer, 1988). Three water masses are involved in this water exchange through the Strait

* Corresponding author at: Departamento de Biología, Facultad de Ciencias del Mar y Ambientales, Universidad de Cádiz, Puerto Real, 11510 Cádiz, Spain.
** Corresponding author at: Departamento de Física, Aplicada, Facultad de Ciencias del Mar y Ambientales, Universidad de Cádiz, Puerto Real, 11510 Cádiz, Spain.
E-mail addresses: iria.sala@gmail.com (I. Sala), marina.bolado@uca.es (M. Bolado-Penagos).

https://doi.org/10.1016/j.jmarsys.2021.103652
Received 1 September 2020; Received in revised form 28 September 2021; Accepted 6 October 2021
Available online 14 October 2021

of Gibraltar: the Surface Atlantic Water (SAW: temperature ~ 22.60 °C and salinity ~ 36.40), the North Atlantic Central Water (NACW: temperature ~ 13.60 °C and salinity ~ 35.80), and the Mediterranean Water (MW: temperature ~ 13.50 °C and salinity ~ 38.40) (Gascard and Richez, 1985; Gómez et al., 2001; Macías et al., 2008b).

The Atlantic Jet (AJ) is the primary driver of the complex circulation of the Alborán Sea (e.g., Bormans and Garrett, 1989; Renault et al., 2012), with an average velocity of ~ 1 m s^{-1} (García-Lafuente et al., 2000). The inflowing jet feeds the quasi-permanent Western Alborán Gyre (WAG; Fig. 1a) and the less intense and persistent Eastern Alborán Gyre (EAG) (e.g., Crepón, 1965; Lacombe, 1971; Lanoix, 1974; Viúdez et al., 1996). Furthermore, the AJ-WAG system breeds a Coastal Cyclonic Gyre (CsCG) that arises close to the Spanish coast (Fig. 1a) and is associated with the upwelling of nutrient-rich waters (Sarhan et al., 2000; Macías et al., 2008a). This scheme, however, is far from being steady. In particular, the frequent occurrence of strong wind events (e.g., Vargas et al., 2003) and the high energetic tidal processes described for this area (e.g., García-Lafuente and Cano, 1994) strongly modify this general pattern (Bolado-Penagos et al., 2021). Briefly, when westerly winds prevail (low sea level pressure over the Mediterranean Sea), the AJ increases its velocity and travels nearer to the Spanish coast (Candela et al., 1990; García-Lafuente et al., 2002b). In this situation, the horizontal extension of the WAG is enhanced, and the CsCG is constrained which reinforces the coastal upwelling (Macías et al., 2008a). In the opposite situation with prevailing winds from the east (high sea level pressure over the Mediterranean Sea), the AJ velocity decreases and travels farther from the Spanish coast (García-Lafuente et al., 1998). This southward displacement of the AJ results in the increase of the horizontal size of the CsCG and the development of an offshore upwelling (Sarhan et al., 2000; Macías et al., 2008a). On the other hand, the high energetic tidal processes that strongly influence the Strait of Gibraltar could also increase/decrease the magnitude of the AJ during the eastward/westward phase of the tidal cycle (e.g., García-Lafuente et al., 2002a; Romero-Cózar et al., 2021). Additionally, tides can destabilize and disengage the AJ-WAG system by enhancing the positive vorticity in the easternmost side of the Strait (Sánchez-Garrido et al., 2013).

In an area as dynamic as the Strait of Gibraltar and the Alborán Sea, biological processes are tightly controlled by hydrodynamics. *In situ* (e.g., Ruiz et al., 2001) and remote sensing studies (e.g., Macías et al., 2007b; Navarro et al., 2011) have revealed enhanced levels of chlorophyll concentration along the AJ related to mesoscale and submesoscale frontal processes. Oguz et al. (2016), using a coupled physical–biological model that did not compute wind forcing nor tidal dynamics, confirmed that the intense frontal activity associated with the Atlantic inflow constitutes a major source of biological enrichment in the Alborán Sea. This is intensified by the tidal cycle that plays an important role in the nutrient supply of the Atlantic water inflow (Macías et al., 2007a; Ramírez-Romero et al., 2014; Sánchez-Garrido et al., 2015). The interaction of the tidal current with the sharp topography of the Strait of Gibraltar generates undulatory features at the Atlantic–Mediterranean Interface (AMI) that modify the AJ properties with a tidal periodicity (e.g., Macías et al., 2006; Bartual et al., 2011; Ramírez-Romero et al., 2012). During spring tides when the AMI is shallower, internal waves lead to the recirculation of nutrients from deep to shallower waters (Wesson and Gregg, 1994; Macías et al., 2007a, 2008a). During neap tides when the interface is deeper, a major contribution of nutrient-enriched NACW is expected (Gómez et al., 2001; Macías et al., 2006). Additionally, the influence of the tidal current could increase the phytoplankton biomass and primary productivity in the Alborán Sea by 40% (Sánchez-Garrido et al., 2015). All of these processes play an important role in the nutrient and biomass input to the Mediterranean Sea which, as previously mentioned, has a natural tendency to oligotrophy.

Previous studies that have focused on the AJ have been performed using satellite imagery (e.g., Macías et al., 2007a; Renault et al., 2012), numerical modelling (e.g., Oguz et al., 2014; Sotillo et al., 2016), and *in situ* data collected with a *Eulerian perspective* (e.g., García-Lafuente et al., 1998; Gómez et al., 2001; Ruiz et al., 2001). There are also a number of studies with a *Lagrangian perspective* that analyse the path followed by the AJ. They are based on the release and monitoring of one or more drifting buoys that can be simple and record only position and time data or more complex and incorporate one or more sensors that record the variables of interest (e.g., temperature) depending on the objective of the study. García-Lafuente and Delgado (2004) analysed the trajectory, the velocity, and the surface temperature (~ 1 m depth) of a mooring array that was accidentally released and was advected with the AJ around the WAG. Vélez-Belchí et al. (2005) released ten neutrally buoyant floats advected with the AJ to provide direct estimates of vertical velocity, temperature, and pressure. Sotillo et al. (2016) used the trajectory followed by several drifting buoys to evaluate the performance of several modelling systems in reproducing the circulation patterns of the Strait of Gibraltar and the Alborán Sea. More recently, Bolado-Penagos et al. (2020) employed Coastal Nomad drifters to characterize the surface circulation patterns from Cape Trafalgar (NW limit of the Strait) towards the Alborán Sea. However, to the best of our knowledge, there is no study that is focused on the AJ with a *Lagrangian perspective* that, in addition to analysing the trajectory followed by the drifter, studies the temporal and spatial evolution of the physical and biological properties along the water column. For that purpose, we have designed a *Lagrangian experiment* that involved the release of a drifter in the Strait of Gibraltar closely followed by an oceanographic vessel on its journey towards the Alborán Sea. The main goals of this study are (i) to describe and analyse in detail the changes in both water attributes and plankton community during this journey and (ii) to infer the physical processes that control the phytoplankton dynamics.

2. Data and methodology

Sampling was conducted during the MEGAN cruise from October 1st to 6th, 2015, on board the R.V. *Sarmiento de Gamboa* during the last days of the spring tide (full moon on September 28th). During this sampling period, a drifting buoy (Offshore Nomad, SouthTEK Sensing Technologies Ltd) with a drogue at ~ 5 m depth was released at the Strait of Gibraltar (5.61 °W – 35.99 °N) to identify the path followed by the inflowing AJ (Fig. 1). The drifter position was obtained from a GPS device, and its position was sent by Iridium satellite communications using the application LDManager (https://ldmanager.southteksl.com). Its position was recorded every ~ 30 min, being possible to estimate its mean velocity from its displacements. The vessel closely followed this drifter, and a sampling station was demarcated each ~ 2 h except at the end of the sampling period when the drifter velocity considerably decreased, and the stations were demarcated every ~ 6 h (stations J43 to J46). On this 110-h journey, a total of 46 sampling stations were carried out (J01 to J46, Fig. 1a) covering a total of 315.62 km (see detailed information in Table A.1).

During the entire cruise, *current-velocity* data were acquired using a vessel-mounted 75-kHz Teledyne RD Instrument Acoustic Doppler Current Profiler Ocean Surveyor. The temporal resolution of these measurements was 60 seconds, and the bin size was 8 m from a 16 to 800 m depth. This database was filtered (i) to exclude those values registered more than 1 km away from the trajectory of the drifter and (ii) to consider only data shallower than 120 m depth. Additionally, to accord with the drifter temporal resolution, the current-velocity data were averaged every 30 minutes.

Wind data were also recorded throughout the entire cruise at the meteorological station on board the research vessel. Wind velocity and direction were recorded every minute. To fit the drifter temporal resolution, both were averaged every 30 minutes.

Temperature, *salinity*, *fluorescence* (previously calibrated to measure chlorophyll in mg m^{-3}) and *photosynthetically active radiation* (PAR)

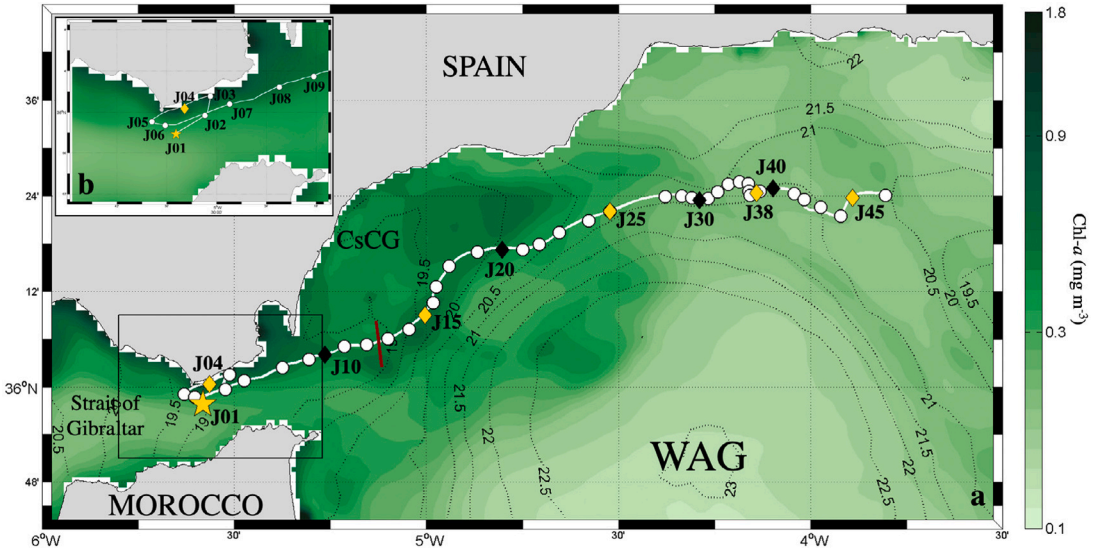

Fig. 1. (a) Location of the different sampling stations (circles) with overlaid mean chlorophyll-*a* concentration (mg m^{-3}) for the sampling period (from October 1st to 6th, 2015). Black dotted contours display the mean sea surface temperature (°C) computed for the sampling period. Both satellite data were downloaded from the Copernicus Marine Environmental Monitoring Service. The black square encloses a (b) zoom of the Strait of Gibraltar region. The white line represents the trajectory followed by the drifting buoy. The star represents the first sampling station of the survey (J01). Yellow diamonds depict the first station of each sampling day (J04, October 2nd; J15, October 3rd; J25, October 4th; J38, October 5th; J35, October 6th). Black diamonds indicate some reference stations (J10, J20, J30 and J40). The red line represents the section analysed in Section 3.3. CsCG: Coastal Cyclonic Gyre. WAG: Western Alborán Gyre.

were recorded down to a depth of 200 m (except for shallower coastal stations J03 and J04, see Table A.1) in each of the 46 sampling stations using a combined CTD probe (Conductivity, Temperature and Depth; Seabird SBE 911 plus). However, only the first 120 m of the water column were analysed which ensured the observation of the AMI boundary that separates the inflowing Atlantic water and the outflowing Mediterranean water. Here, the AMI was associated with the 37.30 isohaline corresponding with the salinity value ascertained at the pycnocline depth from the CTD casts.

From the different temperature and salinity profiles, the *percentage of the NACW* and the *MW* present in the water column were estimated based on a triangulation method following Bray et al. (1995).

Moreover, the *euphotic layer depth* (Z_{eu}) was defined as the depth at which the light intensity was attenuated to 1.00% of the value just below the surface. Thus, Z_{eu} was calculated as:

$$Z_{eu} = \frac{\ln(0.01)}{K_d} \quad (1)$$

where K_d (m^{-1}) is the vertical light attenuation coefficient calculated using the Beer–Lambert Law equation (Kirk, 1994):

$$I_z = I_0 \cdot e^{-K_d \cdot z} \quad (2)$$

where I_z (μEinstein m^{-2} s^{-1}) is the intensity of radiation at any depth, I_0 (μEinstein m^{-2} s^{-1}) is the intensity of radiation at the surface, and z (m) is the depth. Due to the low variability of the PAR in this study, a mean value of Z_{eu} was computed for the whole period considering only the PAR profiles registered during the daylight hours.

Additionally, discrete water samples were collected at each sampling station using a rosette system of 24 Niskin bottles with a volume capacity of 12-L each; this was accomplished at four different depths: 5, ~ 50 and 75 m, and at the Depth of the Chlorophyll Maximum (DCM). The depth limit (i.e., 75 m) was selected considering our interest in studying the inflowing Atlantic water. Several variables related to the dynamics of the pelagic ecosystem were analysed as follows.

For *inorganic nutrients* concentration, two replicates of 5 mL of filtered seawater (0.70 μm Whatman GF/F pre-combusted filters) were collected at each sampling station and depth and stored at -20 °C. Nitrate (NO_3), nitrite (NO_2), and phosphate (PO_4) concentrations were quantified in the laboratory using an autoanalyzer (Technicon AA-II-TRACS 800) following the techniques of Strickland and Parsons (1972).

Samples for the estimation of *pico-* and *nanoplankton* by cytometry were collected at each sampling depth and at all of the stations within the Strait of Gibraltar (J01 to J10) and thereafter only at the odd stations except the last three (J44 to J46) when the jet velocity considerably decreased. Samples were fixed with a solution of 1.00% glutaraldehyde and 0.05% formaldehyde and were immediately counted using a flow cytometer (Becton–Dickinson FacsAria). Laser calibration settings that were employed for the identification of picocyanobacteria and picoeukaryotes were set using natural algae cultures from the microalgae collection of the *Instituto de Ciencias Marinas de Andalucía* (ICMAN-CSIC).

Large nanoplankton and *microplankton* samples (16 to 250 μm) were alternatively collected at odd stations along the entire cruise with the exception of the last three (J44 to J46) at the surface (5 m) and the DCM depths. The analysis of this size fraction was performed on two different water samples. For the smaller fraction (16 - 100 μm), 5 L were filtered and concentrated through a 10-μm mesh to a final volume varying between 100 and 150 mL and subsequently filtered through a 100-μm mesh to discard larger organisms. This fraction was analysed *in vivo*, on board, after water sampling using a FlowCAM® (Fluid Imaging Technologies) to count and measure all organisms. Following the same methodology for the larger fraction (100 – 250 μm), 10 L were filtered and concentrated to a final volume varying between 94 and 134 mL and discarding organisms larger than 250 μm. This fraction was fixed with buffered formaldehyde (4.00% final concentration), stored in amber glass flasks, and later analysed in the laboratory with FlowCAM. For both fractions, the FlowCAM was used in auto-trigger mode (Álvarez et al., 2011) with a chamber of 2.00 mm *x* 0.10 mm and a x10 objective for the smaller fraction and a chamber of 3.00 mm *x* 0.30 mm and a x4 objective for the larger fraction. In both cases, the entire sample was completely processed. The obtained images were sorted automatically applying a neural network with an Inception Resnet v2 architecture (Szegedy et al., 2016) using KERAS (https://keras.io/). Three neural networks based on the size fraction (i.e., cells with a diameter from 16 to 20 μm, 20 to 100 μm, and 100 to 250 μm) were trained to automatically classify the images obtained through the FlowCAM.

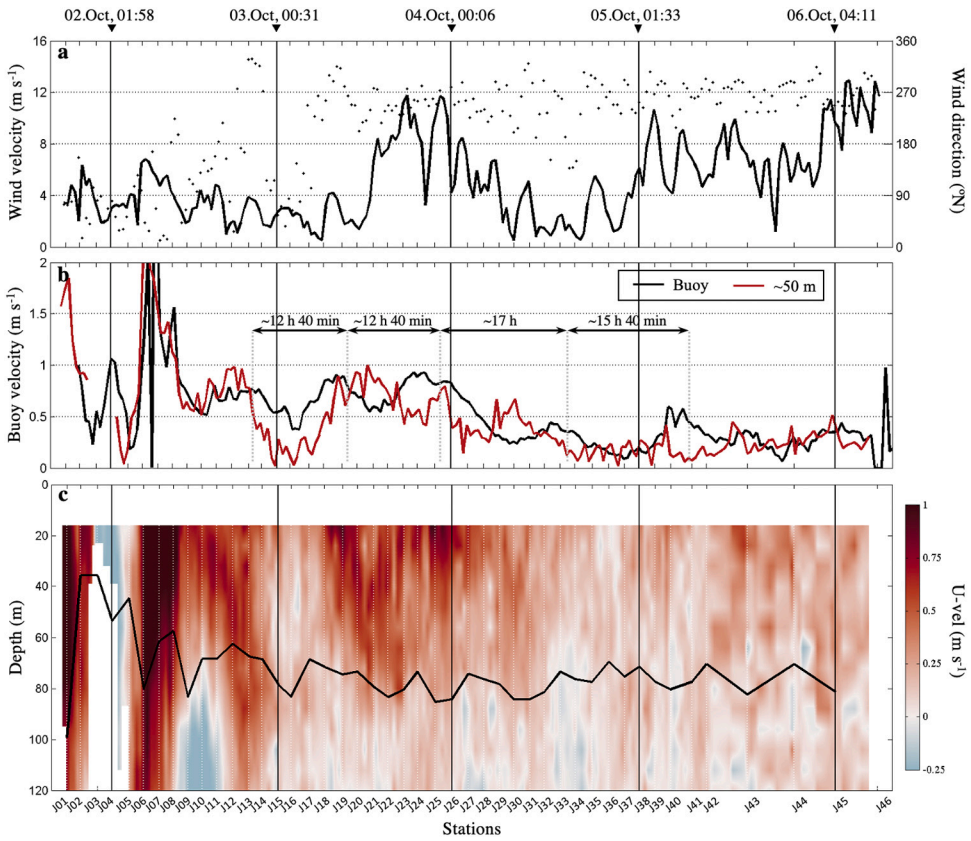

Fig. 2. (a) Temporal evolution of mean wind velocity (m s^{-1}, black line) and direction (°N; black dots) during the entire survey. (b) Temporal evolution of mean drifter velocity (m s^{-1}; black line) and mean current velocity (m s^{-1}) at ~ 50 m depth (red line) during the whole survey. (c) Temporal evolution of the zonal component of the current velocity (u-vel; m s^{-1}) during the entire survey. Positive/negative values indicate the current flows eastward/westward towards the Alborán Sea/Gulf of Cádiz. Black vertical lines represent the first station of each sampling day. The black horizontal line in (c) depicts the Atlantic–Mediterranean Interface (associated with the 37.30 isohaline).

For each neural network, more than 20,000 images were manually classified by an expert to create each training set. Although each set had a different number of categories, in summary, the three size fractions were classified into 29 'functional types' of living particles and three groups of non-living particles (Sala, 2021). The global accuracy of the 16 to 20 μm training set was 71.05% (78.01% for living particles, 66.64% for non-living particles), 72.59% for the 20 to 100 μm training set (75.68% for living particles, 55.39% for non-living particles), and 72.39% for the 100 to 250 μm training set (74.92% for living particles, 70.71% for non-living particles). From a taxonomic perspective, these groups are merged into five 'functional classes' (diatoms, silicoflagellates, dinoflagellates, ciliates, and other unidentified living particles). Each category was associated with a simple geometrical shape thus the individual cell biovolume was calculated using the dimensions (i.e., diameter, length, and width) measured by the FlowCAM software. A previous volume correction was performed for fixed samples (100 - 250 μm) (Menden-Deuer et al., 2001). Total abundance and biovolume at 5 m depth and the DCM were averaged to obtain a mean value for surface layers.

Finally, *mesozooplankton* samples were collected using a Bongo net (mouth opening 0.125 m^2, mesh size 200 μm) by double-oblique tows at odd stations along the entire cruise except the last three (J44 to J46). Samples were collected down to a depth of ~ 75 m (with the exception of the shallower coastal station J03 with 35 m). The net was towed for an average time of 7.16 ± 1.34 minutes at ~ 2 knots, filtering a mean volume of 60.15 ± 8.50 m^3. The retained material was fixed with formaldehyde (4.00% final concentration), stored in plastic bottles, and later analysed in the laboratory. Each mesozooplankton sample was strained onto a 200-μm mesh screen and split to obtain fractions with homogeneous abundances. Subsamples were spilt into a tray manually avoiding overlapping of organisms and photographed with a Nikon D810 camera (36-megapixel sensor) equipped with macro 1:1 lens. Zooplanktonic organisms were counted and measured by image analysis using ImageJ software (https://imagej.nih.gov/ij/). The biovolume of each organism was assumed to be equivalent to that of the corresponding ellipsoid (Jimenez et al., 1987; Alcaraz et al., 2003). A previous volume correction due to shrinkage was performed (Black and Dodson, 2003).

3. Results

3.1. The drifter trajectory

The drifter travelled with an average velocity of 0.51 ± 0.37 m s^{-1} with a maximum value of 3.78 m s^{-1} at the exit of the Strait of Gibraltar (stations J06 to J08) and a minimum < 0.01 m s^{-1} before leaving the Strait (between stations J06 and J07) and in the vicinity of the Djibouti Plateau (J46, Fig. 2b). During the first ~ 10 h of the survey under easterly wind conditions, the drifter described a 360-degree counterclockwise gyre (J01 to J06, Fig. 1b) before leaving the Strait of Gibraltar. From J02 to J04, the zonal component of the current velocity (u-vel) was negative (westward direction) evidencing the entrance of the drifter into the Strait (Fig. 2c). In the next hours, drifter and water column velocity progressively increased and achieved the maximum positive values (eastward direction) of the entire survey (> 2.00 m s^{-1}; J06 to J08, Fig. 2b,c) that drove the drifter out of the Strait. Once the drifter left the Strait, its average velocity did not exceed 1.00 m s^{-1} but varied throughout its journey (Fig. 2b). Between stations J08 and J28, the drifter's average velocity fluctuated between ~ 1.00 and 0.50 m s^{-1} and thereafter fluctuated between ~ 0.50 and < 0.01 m s^{-1} during the

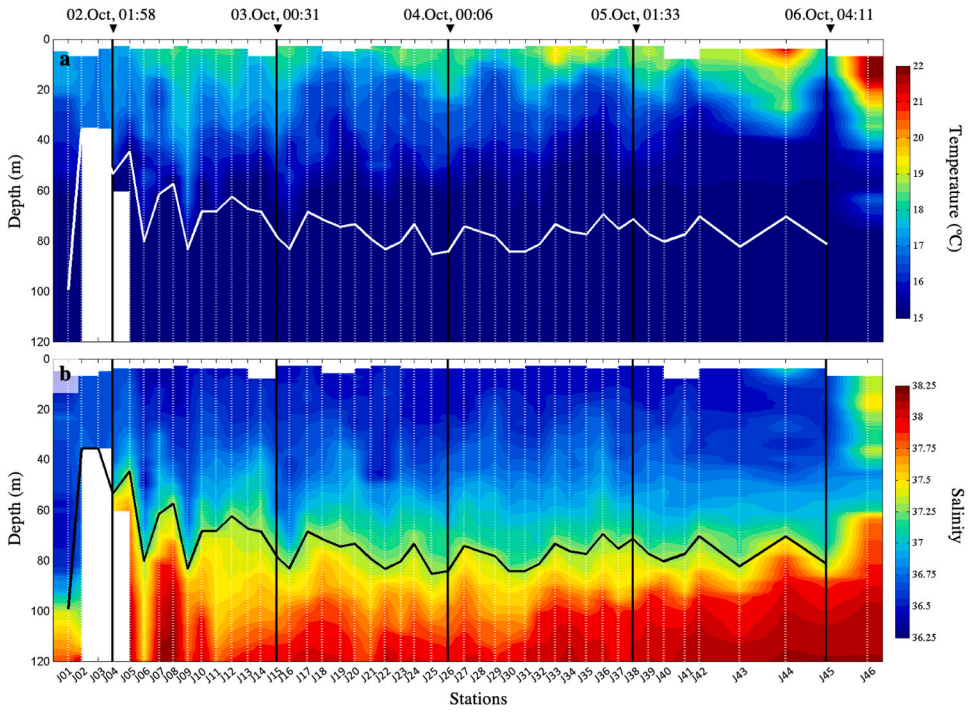

Fig. 3. Temporal evolution of (a) temperature (°C) and (b) salinity during the entire survey. The horizontal line (white in (a) and black in (b)) represents the Atlantic–Mediterranean Interface (associated with the 37.30 isohaline). Black vertical lines indicate the first station of each sampling day. Dotted white lines represent CTD vertical sampling profiles.

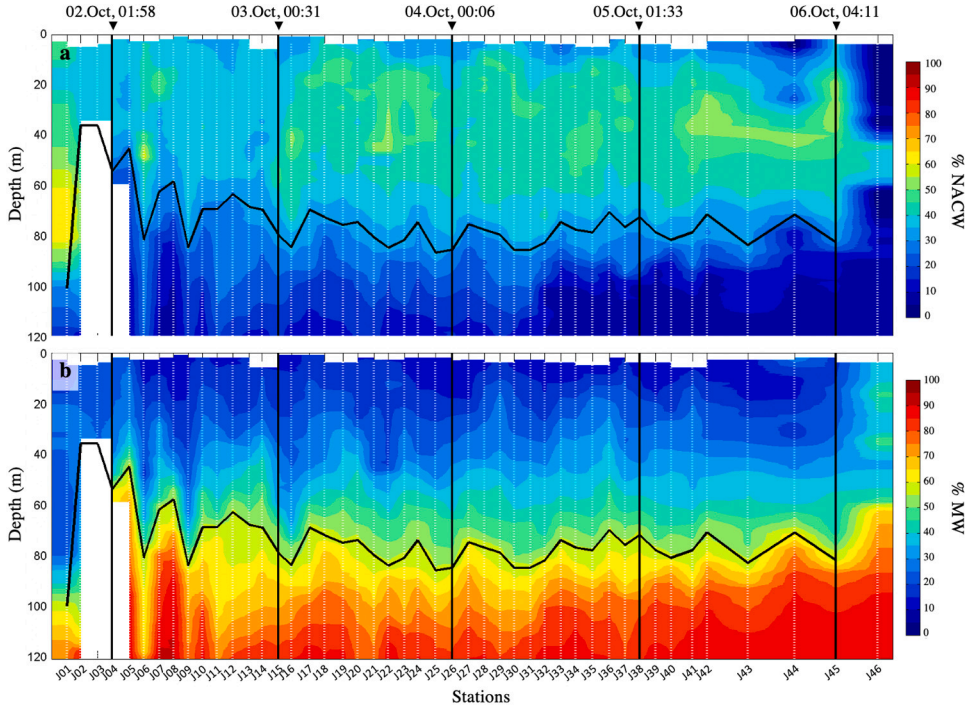

Fig. 4. Temporal evolution of the proportion of (a) North Atlantic Central Water (NACW, %) and (b) Mediterranean Water (MW, %) during the entire survey. The black line represents the Atlantic–Mediterranean Interface (associated with the 37.30 isohaline). Black vertical lines depict the first station of each sampling day. Dotted white lines indicate CTD vertical sampling profiles.

rest of the journey. Five clear peaks of maximum drifter velocity were observed (Fig. 2b). The first three peaks reached maximum values of approximately 1.00 m s^{-1} and the next two had a maximum velocity of ~ 0.50 m s^{-1} (Fig. 2b).

The water column also experienced a progressive decrease in its current velocity along the survey as the drifter moved away from the Strait of Gibraltar. The upper ~ 75 m of the water column (AMI depth = 72.26 ± 13.28 m) corresponding with the inflowing Atlantic water flowed with a mostly positive velocity towards the Alborán Sea (red values, Fig. 2c). Meanwhile, the deepest layer corresponding with the MW flowed with a primarily negative velocity (blue values, Fig. 2c). However, the waving pattern outlined by the drifter velocity was not easily appreciable through the water column. Compared to previous and subsequent values, u-vel between J15 and J18 stations strongly decreased and reached values of < 0.25 m s^{-1}. This zonal velocity

decrease corresponded with an abrupt change in the trajectory of the drifter (Fig. 1a) that mainly moved in a N-NE direction.

3.2. Physical structure of the water column

As the drifter advanced towards the Alborán Sea, the temperature of the inflowing Atlantic water moderately increased, reaching maximum values at the end of the journey (~ 22 °C) while no variation of temperature of the MW was noticeable (< 16 °C; Fig. 3a). On the other hand, the salinity of the inflowing Atlantic water varied little (disregarding J46) but slightly increased on the MW towards the Alborán Sea (Fig. 3b). The temporal evolution of temperature and salinity vertical profiles showed an undulatory pattern from station J10 (outside the Strait) to station J46. This behaviour was also appreciable with the variation of the AMI depth which fluctuated during the whole survey with an average depth of 72.26 ± 13.28 m.

As observed in Fig. 4a, the NACW was mainly distributed in the first 60 – 80 m of the water column with a maximum contribution inside the Strait (> 60%, J01). Once outside the Strait (J11 to J46), its contribution was fairly constant with a mean value of 40.53 ± 2.97%. Although, at several stations, spots with a slightly higher percentage (~ 55%) were observed. Additionally, the percentage of MW demonstrated a progressive increase from the surface to deep waters. Along the first ~ 75 m of the water column, its percentage varied from ~ 5 to 50% close to the AMI (Fig. 4b).

3.3. Physical description of the AJ frontal dynamics

The visual analysis of the u-vel variability along the across-jet section indicated in Fig. 1 (red line), allows identifying the location and width (7.78 km) of the AJ (Fig. 5a) to describe the characteristic frontal dynamics.

Moreover, the across the jet relative vorticity (ζ, s^{-1}) was estimated as:

$$\zeta \equiv v_x - u_y \tag{3}$$

where u and v are the velocity components in x and y (i.e., east and north) directions. ζ was positive (anticlockwise motion) to the north and negative (clockwise motion) to the south (Fig. 5b). ζ reached absolute values as high as $2 \cdot 10^{-4}$ s^{-1}. Consequently, the local Rossby number (R_0, dimensionless) estimated as:

$$R_0 = \frac{\zeta}{f} \tag{4}$$

with f denoting the planetary vorticity (Coriolis parameter, $8.5 \cdot 10^{-5}$ s^{-1} for 36 °N), yields a value of 2.35. With this R_0 value, the jet was prone to lose geostrophic balance. Therefore, to restore this frontal geostrophic balance, a secondary ageostrophic circulation is developed along the across-jet dimension (Mahadevan, 2016).

This secondary ageostrophic circulation is associated with the local increasing of vertical velocity (W, m s^{-1}) along the edges of the jet. Thus, vertical velocity is scaled in accordance to:

$$W \sim R_0 \cdot \delta \cdot U \tag{5}$$

with U being the characteristic current intensity of the jet (u-vel, m s^{-1}) and δ, the small ratio of the Coriolis parameter (f) to the buoyancy frequency (N, s^{-1}), arising from density stratification:

$$\delta = \frac{f}{N} \tag{6}$$

$$N = \sqrt{-\frac{g}{\rho_0} \cdot \frac{d\rho}{dz}} \tag{7}$$

With g being the gravitational acceleration (9.80 m s^{-2}), ρ_0 the initial density of the water mass, and $d\rho/dz$ the relationship between density and depth along the first 100 m of the water column from J10 to J42 (see Fig. A.12), the resulting N has a value of 0.016 s^{-1}.

Considering U = 0.82 m s^{-1} (maximum u-vel along this across section, Fig. 5a) and N = 0.016 s^{-1}, the estimated vertical velocity is as large as 0.01 m s^{-1}. For the AJ, moving eastward, this secondary circulation induces upward/downward vertical velocities in the southern/northern edge of the jet (Mahadevan, 2016).

Another characteristic behaviour of frontal dynamics associated with the secondary ageostrophic circulation is the development of baroclinic instabilities that cause the generation of frontal undulations (i.e., meanders). These meanders reinforce the horizontal density gradients across the jet (isopycnals become closer) intensifying the jet current speed and favouring the loss of the geostrophic balance. For the AJ, flowing eastward, due to vorticity readjustment, a water parcel

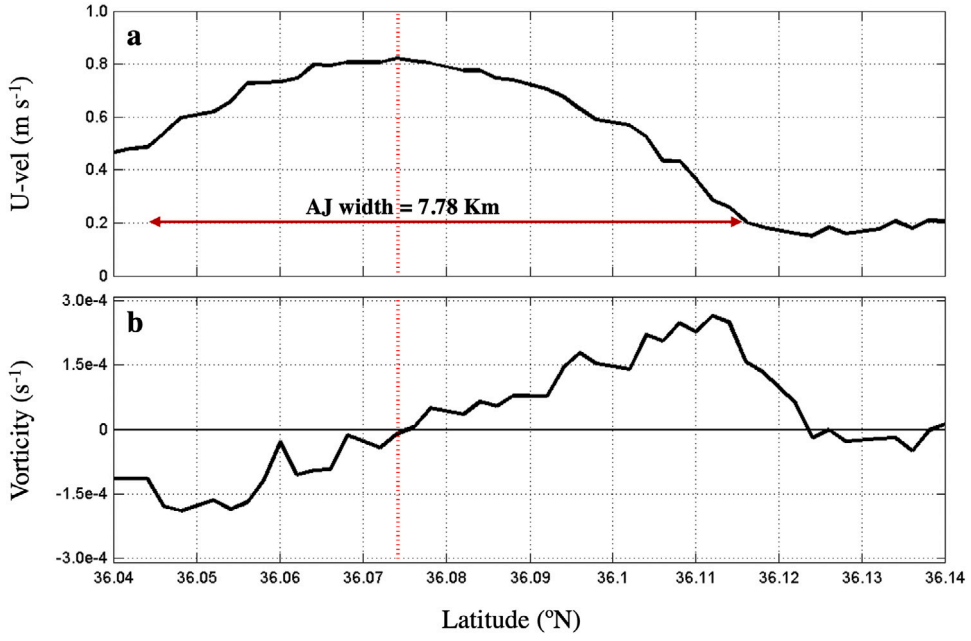

Fig. 5. Latitudinal variation of (a) the zonal component of current velocity (u-vel, m s^{-1}) and (b) the vertical component of relative vorticity (s^{-1}) at 16 m depth along the across-jet section identified in Fig. 1a (red line). The red vertical line identifies the point of maximum u-vel (0.82 m s^{-1}).

moving near the southern edge will tend to be attracted towards the mainstream of the jet when isopycnals are bent to the north and will gain velocity. However, a water parcel will tend to be detached from the jet when the isopycnals are bent to the south and lose velocity (Cushman-Roisin and Beckers, 2011). This behaviour may explain the oscillatory changes in the drifter speed (Fig. 2b); higher/lower drifter speeds would indicate closer/farther distances to the mainstream of the jet.

3.4. Dynamics of nutrients and the pelagic community

To study the dynamics of the water attributes and the pelagic community, we considered the first ~ 75 m of the water column aiming to sample only the inflowing Atlantic water. However, the AMI was regularly observed affecting the deepest water samples at several stations (black horizontal line, Fig. 6).

The $NO_3 + NO_2$ concentration (hereafter NO_x, μM) varied from < 0.01 to ~ 7.00 μM except for station J04 at 25 m depth where the maximum concentration for the entire survey was registered (9.42 μM) (Fig. 6a). As expected, the NO_x increased with depth along the survey with a slight decrease as the drifter advanced in space and time. The analysis of comparative availability of nutrients in surface layers has been made by tracking the position of the NO_x-nutricline depth; the first depth at which the NO_x > 1.00 μM (Fig. 6a; Morán et al., 2001). The first stations in the survey had a clear availability of nutrients (J01 to J10). However, from station J11 onwards, a surface water layer with the NO_x concentration < 1.00 μM was observed (above the white line on Fig. 6a), fluctuating and deepening with time, and achieving its maximum depth at station J44 (~ 35 m depth). This undulating nutrient pattern is associated with the rise of isotherms and isohalines that results in the presence of the NO_x-rich waters in the most superficial layers of the water column. These inputs were less evident at the final stations of the survey.

The PO_4 concentration was clearly higher inside the Strait of Gibraltar at the most coastal stations (J02 to J04, Fig. 6(b) with values of > 0.60 μM. However, once the drifter left the Strait, the PO_4 concentration decreased, varying between < 0.01 and ~ 0.50 μM although with a heterogeneous pattern. The PO_4-nutricline is defined as the first depth at which the PO_4 > 0.10 μM (Morán et al., 2001). In this case, concentration on surface waters reached values of < 0.10 μM PO_4 (above the white line on Fig. 6b) from station J14 onwards. The depth reached by this layer was close to the depth of the euphotic layer (52.66 m) at stations J32 and J45. The PO_4 concentration in the water column considerably decreased from J37 to the end, a fact that could indicate a transition to more oligotrophic waters. The association of the previously described undulatory pattern to the isotherms rising was more difficult to appreciate for the PO_4 except at stations J23, J29, and J35.

Fig. 7 illustrates the temporal evolution of fluorescence on the Atlantic water layer as a proxy for chlorophyll concentration. To more effectively note the undulatory pattern previously observed, mean fluorescence for the first ~ 75 m of the water column is represented in Fig. 7a while, in Fig. 7b, its depth distribution can be examined. Inside the Strait of Gibraltar (J01 to J08), fluorescence was low with mean values of < 0.80 mg m^{-3} except at coastal station J03 with 1.12 mg m^{-3} (Fig. 7a). The vertical distribution of fluorescence showed a higher concentration between stations J12 and J43 in the first ~ 50 m of the water column limited by the euphotic layer (52.66 m) where values between 1.50 and 3.00 mg m^{-3} were recorded (Fig. 7b). During this period (J12 to J43), mean fluorescence described an oscillation with time, although it is from station J19 that the undulatory pattern varied according to the variables previously described (Figs. 3 and 6). However, fluorescence tended to decrease locally when the isotherms ascended, and there was a higher nutrient concentration in shallower layers. Thus, the maximum mean fluorescence peaks and the high fluorescence spots were observed when the isotherms descended and nutrient concentration in surface layers were low. These high fluorescence spots deepened as the drifter progressed into the Alborán Sea, coinciding with the progressive disappearance of the NO_x in surface waters (Figs. 6a and 7b).

The two groups of autotrophic picoplankton analysed in this study showed, as expected, an opposite distribution (see Fig. 8). *Prochlorococcus* was the most abundant group (Fig. 8b) with values of > 10,000 cells mL^{-1} during most of the survey. Several pulses of abundance maxima (> 25,000 cells mL^{-1}) were recorded along the temporal evolution of the water parcel and at different depths (i.e., J06, J21, J23, J25, and J43; Fig. 8a). Some of them (e.g., J25 and J43) coincided with fluorescence maxima (Fig. 7b). *Synechococcus* was the less abundant group with values of ~ 5,000 cells mL^{-1} for almost the entire survey (Fig. 8b). Although, at coastal station J04 and the exit of the Strait of Gibraltar (i.e., J06 to J09), it reached values of ~ 15,000 cells mL^{-1} between 5 and ~ 40 m depth. In the surface waters of J46 station, *Synechococcus* attained its maximum abundance (19,385.54 cells mL^{-1}; Fig. 8b). However, an undulatory pattern similar to that observed for the previous variables was not clearly detected for the two groups of autotrophic picoplankton.

Regarding large-sized phytoplanktonic fractions, diatom abundance was the highest with at least 69% of the total abundance in all sampling stations while its contribution to the total biovolume was > 96% (see Fig. A.13). Thus, hereafter, only the diatoms details are shown. Among the diatoms, the 15 identified categories (Sala, 2021) were classified into six different classes according to their abundance: *Chaetoceros spp.*, *Guinardia spp.*, *Leptocylindrus spp.*, *Skeletonema spp.*, other centric diatoms (i.e., *Thalassiosira spp.*, *Rhizosolenia spp.*), and pennate diatoms (i.e., *Asterionellopsis spp.*, *Pseudo-nitzschia spp.*). The contribution of the different groups to the total diatom population are shown in Fig. 9a. The two most abundant groups were 'other centric diatoms' ranging from 34.37% (J17) to 75.35% (J43) of total diatom abundance and *Chaetoceros spp.*, varying between 8.86% (J43) and 39.56% (J25) (disregarding J01). The contribution of the remaining classes of diatoms varied between quite similar ranges but without a clear trend. Both diatoms' total abundance and biovolume showed a similar trend as the drifter travelled into the Alborán Sea (Fig. 9b) and, as observed previously with other variables, there was an oscillation between minimum and maximum values. Inside the Strait of Gibraltar (J01 to J09), the maximum value of both variables was observed at coastal station J03 (maximum PO_4 concentration, Fig. 6b) with a value ~ 5 times higher than that observed in J01 and ~ 6-times higher than that observed in J07 (minimum value for the entire experiment). Once outside the Strait, the diatom abundance and biovolume continuously increased during the next ~ 20-hours of the survey, achieving the maximum value at J17 (~ 12-folded the initial value). During the remainder of the survey, from J17 to J46, a decreasing trend was observed with two sharp lows at J19 and J46. As previously observed with mean fluorescence, this decreasing trend matches with the progressive disappearance of the NO_x in surface waters (Fig. 6a).

Finally, both mesozooplankton total abundance and biovolume demonstrated the same trend, gradually increasing from the beginning to the end of the *Lagrangian experiment* (Fig. 9c), 4-folding the initial values. This trend showed a series of continuous ups and downs that do not seem to be related to the daily vertical migrations of these organisms.

4. Discussion

To adequately interpret the results obtained in this study, it should be emphasized that the experimental approach did not allow the same water mass to be followed in space and time. Notwithstanding, it did afford us the opportunity to analyse the temporal and spatial evolution of the water properties being introduced through the Strait of Gibraltar with a common origin. Furthermore, it is necessary to take into account that, when the Atlantic water is driven into the Alborán

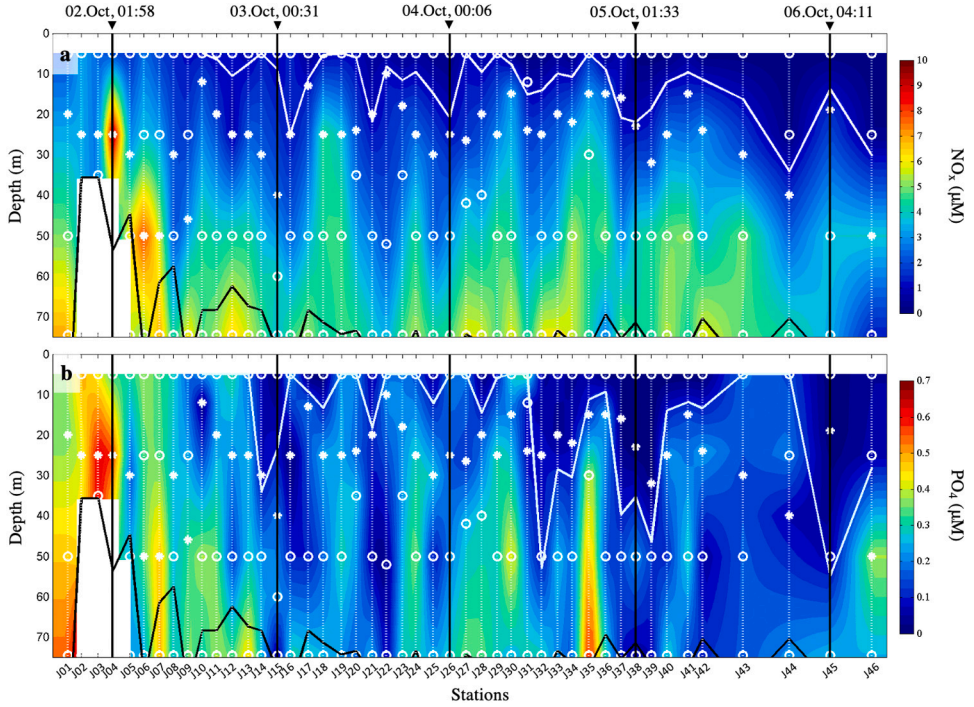

Fig. 6. Temporal evolution of (a) nitrate + nitrite (NO_x), and (b) phosphate (PO_4) concentration (μM) during the entire survey. The black line represents the Atlantic–Mediterranean Interface (associated with the 37.30 isohaline). The white line indicates the minimum depth in which (a) the NO_x concentration is > 1.00 μM, and (b) the PO_4 concentration is > 0.10 μM. Black vertical lines represent the first station of each sampling day. Dotted white lines identify CTD vertical sampling profiles. White circles represent the sampling depths. White asterisks depict the depth of the chlorophyll maximum.

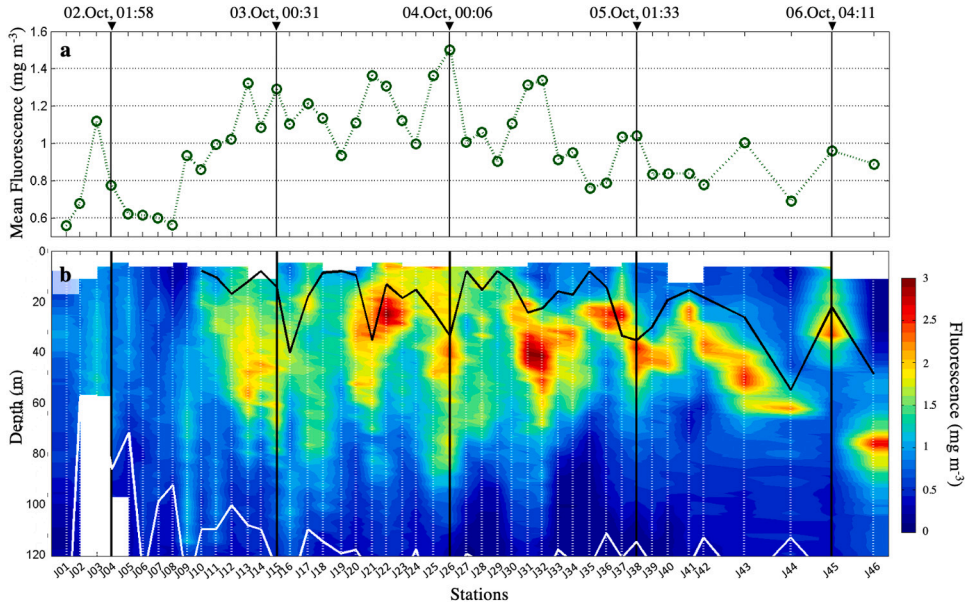

Fig. 7. Temporal evolution of (a) mean fluorescence (mg m^{-3}) computed for the first 75 m of the water column and (b) vertical fluorescence distribution (mg m^{-3}) during the entire survey. Black vertical lines represent the first station of each sampling day. In (b), the white line indicates the Atlantic–Mediterranean Interface (associated with the 37.30 isohaline), the black line signifies the minimum depth in which nitrate + nitrite concentration is > 1.00 μM, and dotted white lines represent CTD vertical sampling profiles.

Sea by the AJ, the intensity of the jet stream decreases significantly with depth (Cushman-Roisin and Beckers, 2011). Consequently, the drifter displacement induced by the jet dynamics will not coincide with those experienced by subsurface water layers. In Fig. 2b, the drifter speed (black line) can be compared with the speed registered at ~ 50 m depth (red line) along the entire study. Within the Strait at both depths (5 and ~ 50 m), the speed was quite similar, however, once in the Alborán Sea, both values differed during the remaining journey. On the other hand, the Atlantic water would be continuously modified by lateral mixing with the surrounding Mediterranean waters. Mixing processes will be more evident along the edges of the jet. Hence, from a combined physical and biochemical perspective, the temporal and spatial evolution of the AJ resembles, to a certain extent, the progression of an upwelling filament: an intrusion of upwelled water into the ocean separated from the surrounding water by fronts (e.g., Wasmund et al., 2016).

Three stages were differentiated according to the most influential processes that induced the temporal and spatial evolution of the physical and biochemical characteristics of the AJ.

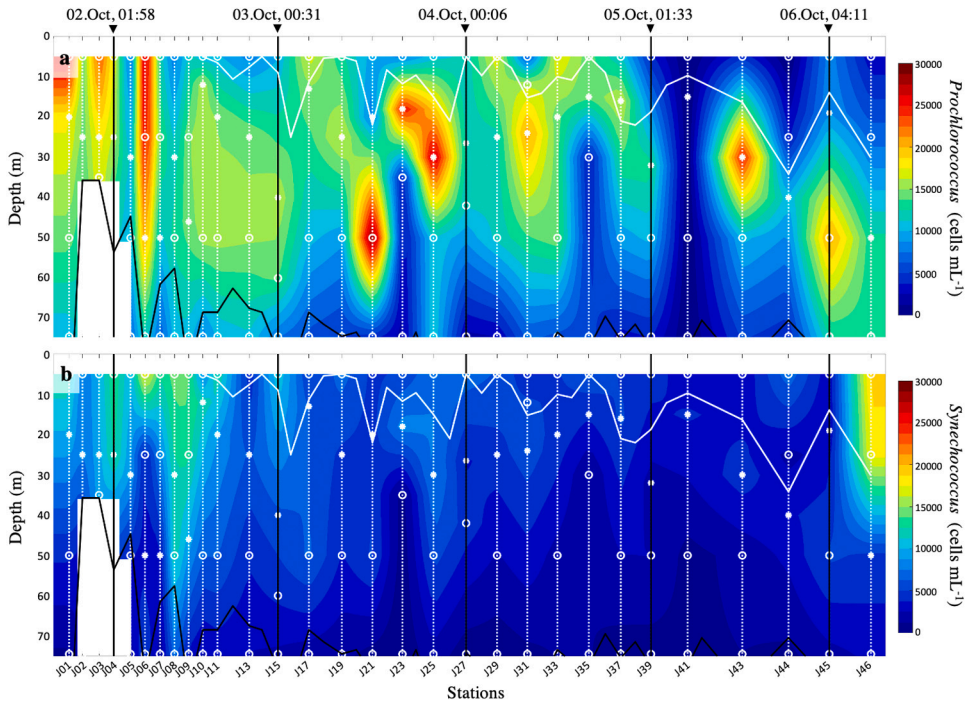

Fig. 8. Temporal evolution of (a) *Prochlorococcus*, and (b) *Synechococcus* abundance (cells mL^{-1}) during the entire survey. The black line represents the Atlantic–Mediterranean Interface (associated with the 37.30 isohaline). The white line indicates the minimum depth in which nitrate + nitrite concentration is > 1.00 μM. Black vertical lines depict the first station of each sampling day. Dotted white lines identify CTD vertical sampling profiles. White circles signify the sampling depths. White asterisks represent the depth of the chlorophyll maximum.

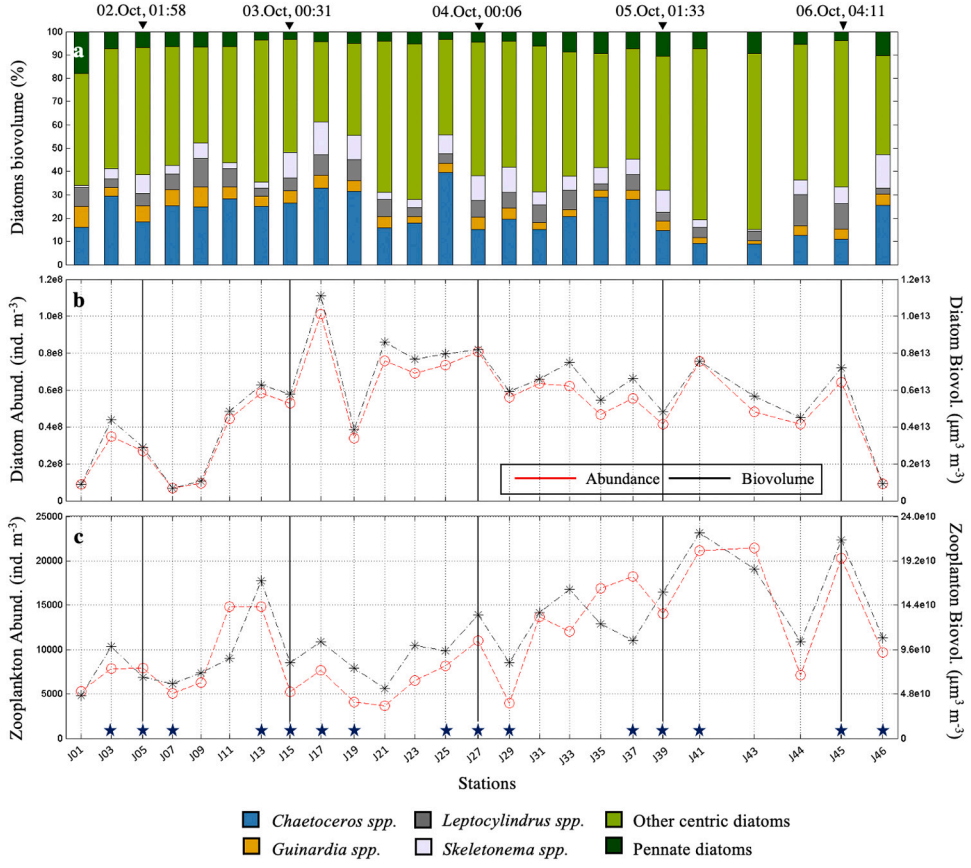

Fig. 9. Temporal evolution of (a) the biovolume composition of the diatom assemblage (%), (b) diatoms total abundance (ind. m^{-3}; red line) and biovolume (μm^{-3} m^{-3}; black line), and (c) zooplankton total abundance (ind. m^{-3}; red line) and biovolume (μm^{-3} m^{-3}; black line) during the entire survey. Black vertical lines in (b) and (c) represent the first station of each sampling day. Black stars in (c) indicate the Bongo samples collected overnight.

4.1. From J01 to J10: Inside the Strait of Gibraltar

This first stage covered from October 1st at 19:51 h to October 2nd at 14:12 h GMT (~ 18 h) while the drifter was inside the Strait of Gibraltar. The 360-degree counterclockwise gyre performed by the drifter (J01 to J06, Fig. 1b) was led by the tidal cycle (data not shown) that moved the drifter towards the Gulf of Cádiz by the westward phase (J03) although easterly winds might also favour this reversion of the inflow (Fig. 2a) (García-Lafuente et al., 2002b). Approximately four hours later, the tidal cycle moved the drifter towards the Alborán Sea by the eastward phase (J05) and thereafter driven out of the Strait by the high increase in the velocity of the water column (J06 to J07, Fig. 2b,c).

Due to the Strait's dynamics that promote the recirculation of nutrients from deep to surface waters and the exchange with coastal waters derived by the counterclockwise gyre (J01 to J06, Fig. 1b), the inflowing Atlantic water, with a 40% – 60% contribution of NACW, began its journey replenished in nutrients. The most intense coastal water exchange appears to occur at J03 when a peak in mean fluorescence was observed (Fig. 7a). Diatoms abundance and biovolume ~ 5-folded their values at this station (J03, Fig. 9b). However, we cannot estimate how much of this population increase was due to the growth population itself and how much to the mixing with the coastal water. From station J01 to J03, there was a time-lapse of ~ 5-hours, therefore, in order to double the diatom cell abundance in this time, their growth rate should be ~ 2.34 day^{-1} (assuming exponential growth under optimal conditions). This value is relatively high compared to the growth rate of 1.59 ± 0.01 day^{-1} for a phytoplankton community obtained in the field experiments by Laws (2013). Additionally, *Chaetoceros spp.* and *Skeletonema spp.*, common coastal diatoms, almost ~ 2-folded and ~ 5-folded their contribution in biovolume, respectively (Fig. 9a). Both of these facts support the mixing with coastal waters.

Finally, when the Atlantic water left the Strait of Gibraltar, it suffered a subduction and a vertical mixing that diluted its properties (station J06, Fig. 3). This vertical dilution was particularly noticeable on nutrient distribution (Fig. 6) and, to a lesser extent, on fluorescence (Fig. 7a). Furthermore, the planktonic community showed a decrease on *Prochlorococcus* and *Synechococcus* cell abundance (Fig. 8) and in diatoms total abundance and biovolume that reached the minimum values of the entire study at J07 (Fig. 9b).

4.2. From J11 to J28: Atlantic Jet - Coastal Cyclonic Gyre Front

This second stage covered from October 2nd at 16:12 h to October 4th at 00:06 h GMT (~ 32 h).

The entrance of the AJ into the Alborán Sea generated a frontal dynamic that has been previously described as a major source of biological enrichment (Oguz et al., 2016). The relatively low saline water of the jet interacting with the more saline water of the Alborán Sea creates a well-marked frontal structure characterized by a strong lateral density gradient. This generates positive (cyclonic) vorticity on the denser side (north of the basin) and negative (anticyclonic) vorticity on the less dense side (towards the centre of the WAG) (see Fig. 5) (Mahadevan, 2016). As previously explained in Section 3.3, the drifter is expected to be influenced by the relative vorticity adjustments experienced by the jet on its adaptation to the meandering of the density front as it is continuously attracted and detached from the most intense stream of the jet (Cushman-Roisin and Beckers, 2011). Hence, a water particle (i.e., the drifter) carried by the AJ will move forward along the jet and laterally across it. The drifter will be attracted to the mainstream along the stretches when the front meanders to the north (i.e., approaching the crest) while it will tend to be detached when the front turns course to the south.

Fig. 10 shows a conceptual diagram of the drifter displacements along and across the jet. In positions 1 and 2 (white circles), the drifter is located at the southern edge of the jet where the current speed is slow, and the water column is characterized by warmer waters. Along this edge, favoured by the low speed, the accumulation of phytoplankton organisms occurs therefore leading to a low nutrient concentration (e.g., Mitchell et al., 2008; Hernández-Carrasco et al., 2018). When the drifter is attracted to the AJ mainstream (position 3 to 5) that is characterized by the highest current speed, it will be surrounded by colder and nutrient-rich waters associated with upwelling processes induced by the intensification of the current (see Section 3.3). Subsequently, the buoy will again become detached from the mainstream moving towards the southern edge where it will travel at a slower speed surrounded by warmer, low-nutrient waters in which phytoplankton accumulates.

Accordingly, along this stage, from J11 to J28, three peaks of maximum drifter speed were observed (Fig. 2b). When the drifter was attracted to the most intense stream of the jet, it progressively increased its speed reaching a maximum value of ~ 1.00 m s^{-1} (Fig. 2b). At the same time that the drifter gained speed, there was also a rise of the isotherms and isohalines observed due to the associated upwelling processes of colder and nutrient-rich NACW and MW (J11, J18 and J23; Figs. 3, 4, and 6). However, when the drifter was detached from the mainstream of the AJ towards the southern edge, its speed slowed down (~ 0.50 m s^{-1}; Fig. 2b), and the isotherms descended (Fig. 3a). Along this edge, the water column was characterized by warmer waters with lower nutrient concentration (J16, J21, J25; Figs. 3a and 6).

Fluorescence values were higher along the southern edge than in the mainstream of the jet (Fig. 7) favoured by the lower speed (e.g., Mitchell et al., 2008; Hernández-Carrasco et al., 2018). Although, along this edge, nutrient concentration was lower probably due to phytoplankton assimilation, there must be an input by horizontal mixing with the adjacent waters (directly influenced by the upwelling processes) that support phytoplankton growth. Additionally, the phytoplankton community located along the edge will be more aged than the one ascertained, at the same time, in the mainstream. For instance, consider two phytoplankton assemblages of similar composition assuming exponential growth under optimal conditions, one travelling on the main flow of the jet at a constant speed of 1.00 m s^{-1} and the second travelling on its edge at 0.50 m s^{-1}. After a certain amount of time, they will both have the same biomass increase, but the assemblage travelling within the mainstream will have advanced twice as far into the Alborán Sea than the one travelling along the edge. Therefore, it is expected that, in the southern edge, if there is no nutrient limitation, the community should exhibit higher fluorescence values (J16, J21, J25; Fig. 7) and have a greater abundance and biomass than the community found at the same time along the mainstream. Notwithstanding, in general, *Prochlorococcus* and *Synechococcus* abundance (Fig. 8) and diatoms total abundance and biovolume (Fig. 9) did not show an oscillation pattern as clearly related with the drifter speed as fluorescence. This lack of coupling with the drifter speed and location could be associated with the fact that plankton samples were collected only in the odd stations, losing temporary resolution.

Along this stage, regardless of the drifter position, mean NO_x concentration in the first 40 m of the water column (deepest DCM) was 2.02 ± 0.16 μM, exceeding the average value of NO_3 half-saturation constant given for the diatoms ($K_s(NO_3)$ = 1.31 ± 0.99 μM, n = 16; value calculated from a literature review, Sala (2021)). Mean PO_4 concentration was 0.23 ± <0.01 μM which is lower (mean value) than the average value of PO_4 half-saturation constant (K_s (PO_4) = 0.75 ± 0.52 μM, n = 6; Sala (2021)). Therefore, the availability of the PO_4 would be limiting for the growth of some diatom species. On the other hand, assuming again an exponential growth under optimal conditions and applying the growth rate of 1.59 day^{-1} for a phytoplankton community (Laws, 2013), the diatom assemblage should have an abundance ~ 4-times lower than that observed in J19. This fact may indicate a punctual interaction with coastal water mass associated with the CsCG (see location of J19 in Fig. 1a). Moreover, although both mesozooplankton total abundance and biovolume increased during this stage (Fig. 9c), it seems that its predatory pressure was not high enough to exert a top-down control over diatoms.

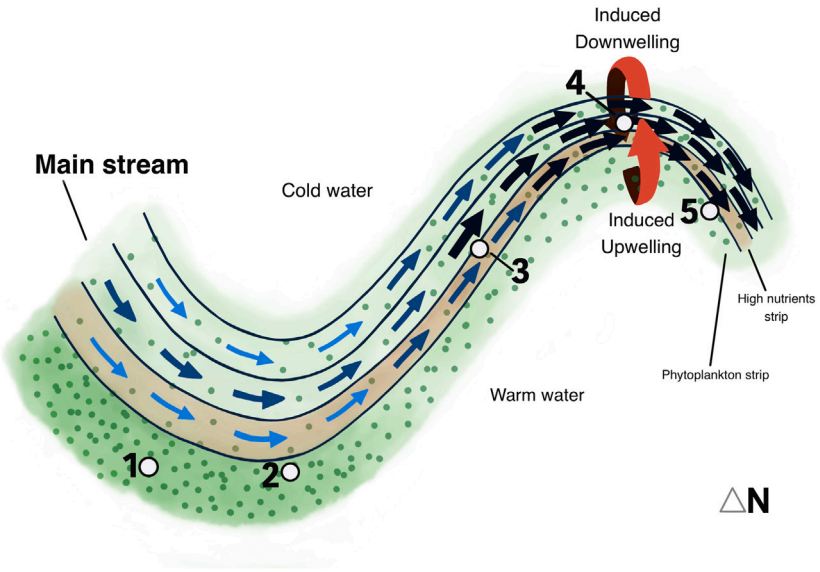

Fig. 10. Conceptual diagram of the drifter displacements along and across the Atlantic Jet. Numbers attached to the white circles indicate the sequential position of the drifter within the jet.

4.3. From J29 to J46: North-Eastern WAG Edge

This third stage covered from October 4th at 02:20 h to October 6th at 09:54 h GMT (~ 56 h). Although this stage lasted half of the total time of the experiment, less than one-third of the total distance was covered (98.62 km) due to the velocity decrease of the drifter as it moved away from the Strait of Gibraltar (Fig. 3b).

Along this stage, two clear peaks of maximum speed were registered when the buoy was attracted to the main stream (from J29 to J42; ~ 0.50 m s^{-1}). These peaks were more separated in time than in the previous stage probably due to the velocity decrease (Fig. 2b). Four upwelling pulses were observed (J29, J35, J41, and J45; Figs. 3 and 6) but not as intense as in the previous stage since the nutrient uplifting did not reach such superficial waters (Fig. 6a). This fact could be also due to a decrease in the drifter velocity as it moved away from the Strait of Gibraltar (Fig. 2b).

Furthermore, during this stage, regardless of the drifter position, the water layer with a NO_x concentration of < 1.00 μM (Fig. 6a) and a PO_4 concentration of < 0.10 μM (Fig. 6b) progressively deepened. This behaviour was also observed for the high fluorescence spots (Fig. 7b). We found that the depth of the water layer with a NO_x concentration of < 1.00 μM and the DCM (fluorescence), showed a positive correlation ($r = 0.76$, $p < 0.001$, $n = 20$). Two processes could explain this trend: (i) a vertical displacement of the phytoplankton community to subsurface layers as a biological response to naturally nutrient-depleted superficial layers; and/or (ii) the physical sinking of the colder and denser AJ as it moves surrounded by warmer waters (see Fig. 1a). This second process was previously observed in filaments (Sánchez et al., 2008; Cravo et al., 2010) and is also responsible for the deepening of the phytoplankton community.

To verify the physical sinking of the AJ, we have analysed the position of the DCMs (fluorescence) against density from stations J29 to J46 down to 75 m depth. Hence, if the deepening of DCMs is linked with a certain isopycnal, the jet subduction is taking place. Fig. 11 illustrates the positive correlation found between the DCMs and the density range 26.60 – 26.80 kg m^{-3} (corresponding to NACW). The strongest positive correlation was determined for the 26.70 kg m^{-3} isopycnal ($r = 0.87$, $p < 0.001$, $n = 18$). The same analysis for the previous stage (J11 to J28) showed a lower correlation ($r = 0.57$; $p < 0.05$; $n = 18$) probably evidencing a strongest influence of the submesoscale instabilities. Previous studies in the region have already shown a clear correlation between the DCM and a certain isopycnal (Navarro et al., 2006; Macías et al., 2008b; Navarro and Ruiz, 2013; Olita et al., 2017).

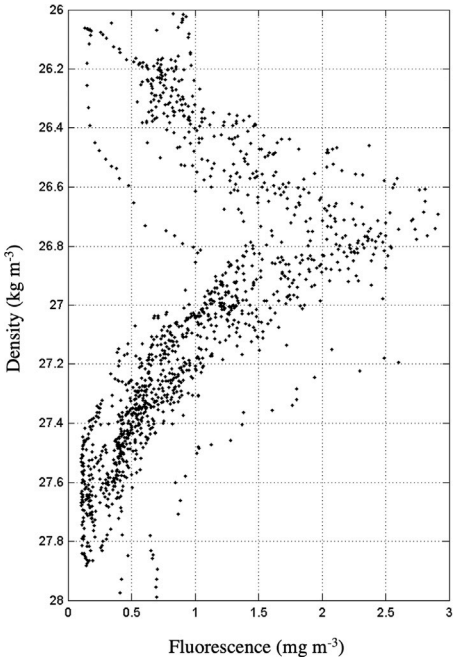

Fig. 11. Density (kg m^{-3}) versus fluorescence (mg m^{-3}) profiles from station J29 to J46 until 75 m depth.

Concomitantly and regardless of the drifter position, fluorescence, *Prochlorococcus* and *Synechococcus* abundance, and diatoms total abundance and biovolume began to progressively decrease (Figs. 7, 8,

and 9b). This fact could be caused by the decrease in nutrient availability and/or the increase of mesozooplankton total abundance and biovolume (Fig. 9c).

5. Conclusions

Our *Lagrangian experiment* evidenced a strong control of the physical environment on the ecological processes throughout the entire studied period. Inside the Strait of Gibraltar, the inflowing Atlantic water was primarily influenced by the tidal cycle. Once in the Alborán Sea, it was mainly influenced by the frontal dynamics associated with the AJ.

Diatoms dominated the phytoplankton community, corroborating their importance as main primary producers in the Strait and evidencing their adaptability to physical derived changes, obtaining an advantage over other microplanktonic groups. These diatom assemblages increased in cell abundance throughout the experiment but did not demonstrate a significant successional change since the percentage of each group remained relatively constant. This fact could highlight that the inflowing Atlantic water continuously evolved surrounded by water with similar properties and a common origin, however, the sampling period was not long enough to appreciate a change in the community composition or even a decrease in the diatom total abundance or biovolume.

Nevertheless, the development of the AJ (i.e., velocity, entering angle) depends on the combination of different processes such as meteorological forcing, seasonal variability, the wind regime, and the tidal cycle. Thus, the properties that characterize the Atlantic water that leaves the Strait may differ (i.e., mean temperature and salinity or nutrient budget). Consequently, from a biological perspective, there should be a wide variety of different situations to that presented in this work. In fact, Macías et al. (2008a) found that the composition and nature of the phytoplankton assemblage that leaves the Strait depends on water masses' interaction and interfaces. Thus, new *Lagrangian experiments* under different conditions (particularly considering the tidal cycle) would be of significant interest.

CRediT authorship contribution statement

Iria Sala: Processed the experimental data, Implemented the neural networks, Accomplished the data analysis, Writing – original draft, Writing – review & editing. **Marina Bolado-Penagos:** Processed the experimental data, Accomplished the data analysis, Writing – review & editing. **Ana Bartual:** Designed the study, Accomplished the data analysis, Writing – review & editing. **Miguel Bruno:** Designed the study, Accomplished the data analysis, Writing – review & editing. **Carlos M. García:** Designed the study, Accomplished the data analysis, Writing – review & editing. **Ángel López-Urrutia:** Implemented the neural networks, Writing – review & editing. **Cristina González-García:** Processed the experimental data, Writing – review & editing. **Fidel Echevarría:** Designed the study, Accomplished the data analysis, Writing – review & editing.

Declaration of competing interest

The authors declare that they have no known competing financial interests or personal relationships that could have appeared to influence the work reported in this paper.

Acknowledgements

The authors gratefully acknowledge the officers, crew and technical staff of the R.V. *Sarmiento de Gamboa* for their altruistic help during the cruise, all the scientific team that participated in the MEGAN campaign collecting the different datasets, Manuel Arjonilla for nutrient sample measurements, and Reyes García for her collaboration in the treatment of plankton samples. They also thank the Copernicus Marine Environmental Monitoring Service for providing access to satellite data. Neural network analyses were performed in the facilities of the *Área de Sistemas de Información de la Universidad de Cádiz* (https://supercomputacion.uca.es). Finally, the authors acknowledge Sara Soria Píriz (@nautillustrations) for the drawing of the conceptual diagram in Fig. 10. Comments provided by two anonymous reviewers substantially improved subsequent versions of the manuscript. The Spanish National Research Plan through project CTM2013-49048 has supported this work. Iria Sala and Marina Bolado-Penagos were supported by a grant of the FPI fellowship program, Spain. To accomplish this work, Iria Sala carried out a short-term stay with the research group *Dinámica del Ecosistema Planctónico* at the *Instituto Español de Oceanografía de Gijón*, under the supervision of Dr Ángel López-Urrutia, supported by a grant of the FPI fellowship program.

Appendix A

See Table A.1, Figs. A.12 and A.13.

Table A.1
Summary of the sampling stations performed during the *Lagrangian experiment*.

Station	Time (GMT)	Lat (°N)	Lon (°W)	Depth (m)	Distance (km)
J01	01.10.2015 - 19:51	35.96	5.58	664.98	0.00
J02	01.10.2015 - 21:41	35.99	5.52	464.34	9.10
J03	01.10.2015 - 23:57	36.03	5.51	38.29	10.80
J04	02.10.2015 - 01:58	36.01	5.56	66.12	18.91
J05	02.10.2015 - 04:17	35.99	5.63	195.89	29.21
J06	02.10.2015 - 06:16	35.98	5.60	398.61	33.38
J07	02.10.2015 - 08:20	36.01	5.47	436.18	53.68
J08	02.10.2015 - 10:18	36.04	5.37	525.83	69.35
J09	02.10.2015 - 12:15	36.06	5.31	832.78	80.21
J10	02.10.2015 - 14:12	36.07	5.26	861.64	86.69
J11	02.10.2015 - 16:12	36.09	5.21	820.17	94.49
J12	02.10.2015 - 18:19	36.09	5.15	837.79	103.77
J13	02.10.2015 - 20:34	36.10	5.10	807.69	112.47
J14	02.10.2015 - 22:19	36.12	5.05	821.54	120.94
J15	03.10.2015 - 00:31	36.15	5.00	828.54	127.58
J16	03.10.2015 - 02:16	36.18	4.98	811.33	130.88
J17	03.10.2015 - 04:45	36.21	4.97	737.40	132.18
J18	03.10.2015 - 06:46	36.25	4.94	620.31	137.48
J19	03.10.2015 - 09:17	36.28	4.87	679.18	148.81
J20	03.10.2015 - 11:16	36.29	4.80	759.36	159.02
J21	03.10.2015 - 13:29	36.29	4.75	795.92	167.54
J22	03.10.2015 - 15:26	36.30	4.71	785.27	174.09
J23	03.10.2015 - 17:36	36.32	4.66	864.23	182.23
J24	03.10.2015 - 19:27	36.35	4.58	707.67	194.36
J25	03.10.2015 - 21:51	36.37	4.52	653.17	203.07
J26	04.10.2015 - 00:06	36.39	4.43	591.71	217.00
J27	04.10.2015 - 02:20	36.40	4.38	573.08	225.68
J28	04.10.2015 - 04:28	36.40	4.34	580.41	232.37
J29	04.10.2015 - 06:35	36.40	4.31	630.39	236.49
J30	04.10.2015 - 08:33	36.39	4.29	621.06	239.55
J31	04.10.2015 - 10:44	36.40	4.27	629.03	243.32
J32	04.10.2015 - 12:41	36.41	4.24	623.05	247.14
J33	04.10.2015 - 14:51	36.42	4.21	654.16	251.44
J34	04.10.2015 - 16:50	36.43	4.19	638.01	255.93
J35	04.10.2015 - 19:10	36.43	4.16	659.57	259.53
J36	04.10.2015 - 21:26	36.41	4.16	681.40	259.77
J37	04.10.2015 - 23:34	36.40	4.16	691.04	260.29
J38	05.10.2015 - 01:33	36.41	4.14	694.92	263.03
J39	05.10.2015 - 03:42	36.41	4.13	695.40	264.48
J40	05.10.2015 - 05:50	36.42	4.10	707.32	269.60
J41	05.10.2015 - 08:44	36.40	4.04	737.32	278.38
J42	05.10.2015 - 10:41	36.39	4.09	512.30	282.36
J43	05.10.2015 - 16:15	36.38	3.97	330.78	289.18
J44	05.10.2015 - 22:35	36.36	3.92	749.01	297.31
J45	06.10.2015 - 04:11	36.40	3.89	772.14	302.28
J46	06.10.2015 - 09:54	36.40	3.81	887.40	315.62

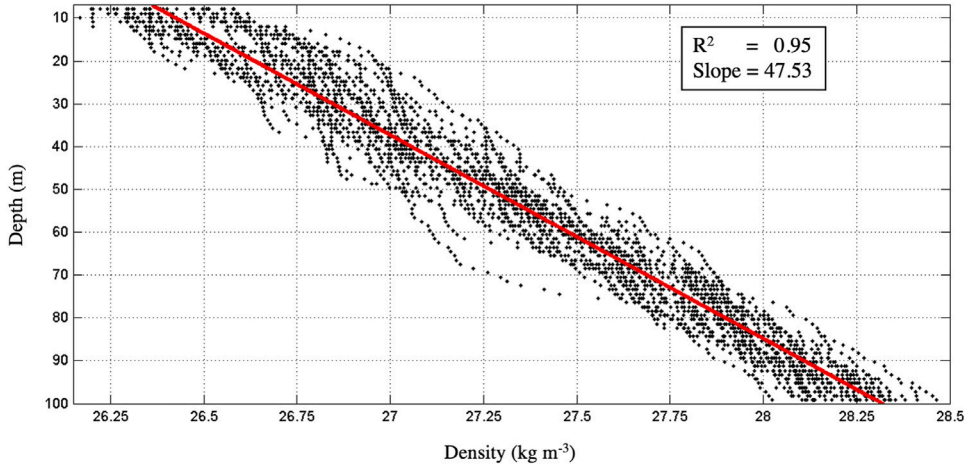

Fig. A.12. Relationship between depth (m) and density (kg m^{-3}) along the first 100 m of the water column for stations J10 to J42.

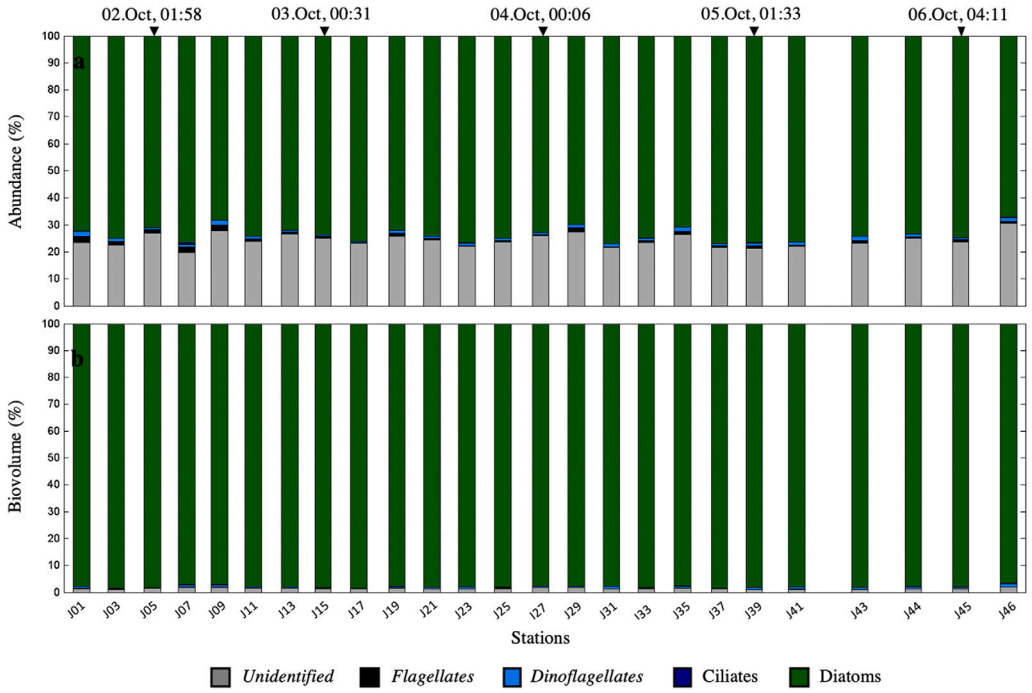

Fig. A.13. Microplankton community composition: (a) abundance (%), and (b) biovolume (%).

References

Alcaraz, M., Saiz, E., Calbet, A., Trepat, I., Broglio, E., 2003. Estimating zooplankton biomass through image analysis. Mar. Biol. 143, 307–315. http://dx.doi.org/10.1007/s00227-003-1094-8.

Álvarez, E., López-Urrutia, Á., Nogueira, E., Fraga, S., 2011. How to effectively sample the plankton size spectrum? A case study using FlowCAM. J. Plankton Res. 33, 1119–1133. http://dx.doi.org/10.1093/plankt/fbr012.

Armi, L., Farmer, D.M., 1988. The flow of Mediterranean water through the Strait of Gibraltar. Prog. Oceanogr. 21, 1–103. http://dx.doi.org/10.1016/0079-6611(88)90055-9.

Bartual, A., Macías, D., Gutiérrez-Rodríguez, A., García, C.M., Echevarría, F., 2011. Transient pulses of primary production generated by undulatory processes in the western sector of the Strait of Gibraltar. J. Mar. Syst. 87, 25–36. http://dx.doi.org/10.1016/j.jmarsys.2011.02.021.

Black, A.R., Dodson, S.I., 2003. Ethanol: a better preservation technique for Daphnia. Limnol. Oceanogr.: Methods 1, 45–50. http://dx.doi.org/10.4319/lom.2011.1.45.

Bolado-Penagos, M., González, C.J., Chioua, J., Sala, I., Gomiz-Pascual, J.J., Vázquez, Á., Bruno, M., 2020. Submesoscale processes in the coastal margins of the Strait of Gibraltar. The Trafalgar – Alboran connection. Prog. Oceanogr. 102219. http://dx.doi.org/10.1016/j.pocean.2019.102219.

Bolado-Penagos, M., Sala, I., Gomiz-Pascual, J.J., Romero-Cózar, J., González-Fernández, D., Reyes-Pérez, J., Vázquez, Á., Bruno, M., 2021. Revising the effects of local and remote atmospheric forcing on the Atlantic Jet and Western Alboran Gyre dynamics. J. Geophys. Res. Oceans 126, http://dx.doi.org/10.1029/2020jc016173.

Bormans, M., Garrett, C., 1989. A simple criterion for gyre formation by the surface outflow from a strait, with application to the Alborán Sea. J. Geophys. Res. 94, 12637–12644.

Bray, N., Ochoa, J., Kinder, T., 1995. The role of the interface in exchange through the Strait of Gibraltar. J. Geophys. Res. 100, 10755–10776. http://dx.doi.org/10.1029/95JC00381.

Candela, J., Winant, C., Ruiz, A., 1990. Tides in the Strait of Gibraltar. J. Geophys. Res. 95, 7313–7335.

Cravo, A., Relvas, P., Cardeira, S., Rita, F., Madureira, M.S., 2010. An upwelling filament off southwest Iberia: Effect on the chlorophyll-a and nutrient export. Cont. Shelf Res. 30, 1601–1613. http://dx.doi.org/10.1016/j.csr.2010.06.007.

Crepón, M., 1965. Influence de la pression atmosphérique sur le niveau moyen de la Méditerranée occidentale et sur le flux à travers le détroit de Gibraltar. Cah. Océanograph. 17, 15–32.

Cushman-Roisin, B., Beckers, J.M., 2011. Geostrophic flows and vorticity dynamics. In: Cushman-Roisin, B., Beckers, J.M. (Eds.), International Geophysics. Academic Press, pp. 205–238. http://dx.doi.org/10.1016/B978-0-12-088759-0.00007-9, (Chapter 7).

García-Lafuente, J., Cano, N., 1994. Tidal dynamics and associated features of the northwestern shelf of the Alboran Sea. Cont. Shelf Res. 14, 1–21. http://dx.doi.org/10.1016/0278-4343(94)90002-7.

García-Lafuente, J., Cano, N., Vargas, M., Rubín, J.P., Hernández-Guerra, A., 1998. Evolution of the Alboran Sea hydrographic structures during July 1993. Deep-Sea Res. I 45, 39–65. http://dx.doi.org/10.1016/S0967-0637(97)00216-1.

García-Lafuente, J., Delgado, J., 2004. The meandering path of a drifter around the western Alborán Gyre. J. Phys. Oceanogr. 34, 685–692. http://dx.doi.org/10.1175/3516.1.

García-Lafuente, J., Delgado, J., Criado, F., 2002a. Inflow interruption by meteorological forcing in the Strait of Gibraltar. Geophys. Res. Lett. 29, 20–1–20–4. http://dx.doi.org/10.1029/2002gl015446.

García-Lafuente, J., Delgado, J., Vargas, J.M., Vargas, M., Plaza, F., Sarhan, T., 2002b. Low-frequency variability of the exchanged flows through the Strait of Gibraltar during CANIGO. Deep-Sea Res. II 49, 4051–4067.

García-Lafuente, J., Vargas, J.M., Plaza, F., 2000. Tide at the eastern section of the Strait of Gibraltar. J. Geophys. Res. 105, 14197–14213. http://dx.doi.org/10.1029/2000JC900007.

Gascard, J., Richez, C., 1985. Water masses and circulation in the Western Alboran sea and in the Straits of Gibraltar. Prog. Oceanogr. 15, 157–216. http://dx.doi.org/10.1016/0079-6611(85)90031-X.

Gómez, F., Gorsky, G., Striby, L., Vargas, J.M., González, N., Picheral, M., García-Lafuente, J., Varela, M., Goutx, M., 2001. Small-scale temporal variations in biogeochemical features in the Strait of Gibraltar, Mediterranean side - The role of NACW and the interface oscillation. J. Mar. Syst. 30, 207–220. http://dx.doi.org/10.1016/S0924-7963(01)00059-8.

Hernández-Carrasco, I., Orfila, A., Rossi, V., Garçon, V., 2018. Effect of small scale transport processes on phytoplankton distribution in coastal seas. Sci. Rep. 8, 8613. http://dx.doi.org/10.1038/s41598-018-26857-9.

Jimenez, F., Rodríguez, J., Bautista, B., Rodríguez, V., 1987. Relations between chlorophyll, phytoplankton cell abundance and biovolume during a winter bloom in Mediterranean coastal waters. J. Exp. Mar. Biol. Ecol. 105, 161–173. http://dx.doi.org/10.1016/0022-0981(87)90169-9.

Kirk, J.T.O., 1994. Light and Photosynthesis in Aquatic Ecosystems, second ed. Cambridge University Press, http://dx.doi.org/10.1017/CBO9780511623370.

Lacombe, H., 1971. Le Dètroit de Gibraltar; Oceanographique Physique. In: Mèmorie explicatif de la carte gèotechnique de Tanger au 1/250000, 222, pp. 111e146. In: Notes et Mém. Serv. Gèologique. Maroc. Notes et Mém. Serv. Gèologique. Maroc. 222. p. 111e116.

Lanoix, F., 1974. Etude hydrologique et dynamique de la mer d'Alboran. North Atlantic Treaty, p. 66.

Laws, E.A., 2013. Evaluation of in situ phytoplankton growth rates: A synthesis of data from varied approaches. Annu. Rev. Mar. Sci. 5, 247–268. http://dx.doi.org/10.1146/annurev-marine-121211-172258.

Macías, D., Bruno, M., Echevarría, F., Vázquez, Á., García, C.M., 2008a. Meteorologically-induced mesoscale variability of the North-Western Alboran Sea (southern Spain) and related biological patterns. Estuar. Coast. Shelf Sci. 78, 250–266. http://dx.doi.org/10.1016/j.ecss.2007.12.008.

Macías, D., García, C.M., Echevarría, F., Vázquez, Á., Bruno, M., 2006. Tidal induced variability of mixing processes on Camarinal Sill (Strait of Gibraltar): A pulsating event. J. Mar. Syst. 60, 177–192. http://dx.doi.org/10.1016/j.jmarsys.2005.12.003.

Macías, D., Lubián, L.M., Echevarría, F., Huertas, I.E., García, C.M., 2008b. Chlorophyll maxima and water mass interfaces: Tidally induced dynamics in the Strait of Gibraltar. Deep-Sea Res. I 55, 832–846. http://dx.doi.org/10.1016/j.dsr.2008.03.008.

Macías, D., Martin, A.P., García-Lafuente, J., García, C.M., Yool, A., Bruno, M., Vázquez, Á., Izquierdo, A., Sein, D., Echevarría, F., 2007a. Analysis of mixing and biogeochemical effects induced by tides on the Atlantic-Mediterranean flow in the Strait of Gibraltar through a physical-biological coupled model. Prog. Oceanogr. 74, 252–272. http://dx.doi.org/10.1016/j.pocean.2007.04.006.

Macías, D., Navarro, G., Echevarría, F., García, C.M., Cueto, J., 2007b. Phytoplankton pigment distribution in the northwestern Alborán Sea and meteorological forcing: A remote sensing study. J. Mar. Res. 65, 523–543. http://dx.doi.org/10.1357/002224007782689085.

Mahadevan, A., 2016. The impact of submesoscale physics on primary productivity of plankton. Annu. Rev. Mar. Sci. 8, 17.1–17.24. http://dx.doi.org/10.1146/annurev-marine-010814-015912.

Menden-Deuer, S., Lessard, E.J., Satterberg, J., 2001. Effect of preservation on dinoflagellate and diatom cell volume and consequences for carbon biomass predictions. Mar. Ecol. Prog. Ser. 222, 41–50. http://dx.doi.org/10.3354/meps222041.

Mitchell, J.G., Yamazaki, H., Seuront, L., Wolk, F., Li, H., 2008. Phytoplankton patch patterns: Seascape anatomy in a turbulent ocean. J. Mar. Syst. 69, 247–253. http://dx.doi.org/10.1016/j.jmarsys.2006.01.019.

Morán, X.A.G., Taupier-Letage, I., Vázquez-Domínguez, E., Ruiz, S., Arin, L., Raimbault, P., Estrada, M., 2001. Physical-biological coupling in the algerian basin (sw mediterranean): Influence of mesoscale instabilities on the biomass and production of phytoplankton and bacterioplankton. Deep Sea Res. I 48, 405–437. http://dx.doi.org/10.1016/S0967-0637(00)00042-X.

Navarro, G., Ruiz, J., 2013. Hysteresis conditions the vertical position of deep chlorophyll maximum in the temperate ocean. Glob. Biogeochem. Cycles 27, 1013–1022. http://dx.doi.org/10.1002/gbc.20093.

Navarro, G., Ruiz, J., Huertas, I.E., García, C.M., Criado-Aldeanueva, F., Echevarría, F., 2006. Basin-scale structures governing the position of the deep fluorescence maximum in the Gulf of Cádiz. Deep-Sea Res. II 53, 1261–1281. http://dx.doi.org/10.1016/j.dsr2.2006.04.013.

Navarro, G., Vázquez, Á., Macías, D., Bruno, M., Ruiz, J., 2011. Understanding the patterns of biological response to physical forcing in the Alborán Sea (western Mediterranean). Geophys. Res. Lett. 38, 1–5. http://dx.doi.org/10.1029/2011GL049708.

Oguz, T., Macías, D., García-Lafuente, J., Pascual, A., Tintoré, J., 2014. Fueling plankton production by a meandering frontal jet: A case study for the Alborán sea (Western Mediterranean). PLoS One 9, http://dx.doi.org/10.1371/journal.pone.0111482.

Oguz, T., Mourre, B., Tintoré, J., 2016. Upstream control of the frontal jet regulating plankton production in the Alboran Sea (Western Mediterranean). J. Geophys. Res. Oceans 121, http://dx.doi.org/10.1002/2015JC011486.Received.

Olita, A., Capet, A., Claret, M., Mahadevan, A., Poulain, P.M., Ribotti, A., Ruiz, S., Tintoré, J., Tovar-Sánchez, A., Pascual, A., 2017. Frontal dynamics boost primary production in the summer stratified Mediterranean Sea. Ocean Dyn. 67, 767–782. http://dx.doi.org/10.1007/s10236-017-1058-z.

Ramírez-Romero, E., Macías, D., Bruno, M., Reyes, E., Navarro, G., García, C.M., 2012. Submesoscale, tidally-induced biogeochemical patterns in the Strait of Gibraltar. Estuar. Coast. Shelf Sci. 101, 24–32. http://dx.doi.org/10.1016/j.ecss.2012.02.010.

Ramírez-Romero, E., Macías, D., García, C.M., Bruno, M., 2014. Biogeochemical patterns in the Atlantic Inflow through the Strait of Gibraltar. Deep-Sea Res. I 85, 88–100. http://dx.doi.org/10.1016/j.dsr.2013.12.004.

Renault, L., Oguz, T., Pascual, A., Vizoso, G., Tintoré, J., 2012. Surface circulation in the Alborán Sea (western Mediterranean) inferred from remotely sensed data. J. Geophys. Res. Oceans 117, 1–11. http://dx.doi.org/10.1029/2011JC007659.

Romero-Cózar, J., Chioua, J., Bolado-Penagos, M., Reyes-Pérez, J., Gomiz-Pascual, J.J., Vázquez, Á., Sirviente, S., Bruno, M., 2021. Tidally-induced submesoscale features in the atlantic jet and Western Alboran Gyre. A study based on HF radar and satellite images. Estuar. Coast. Shelf Sci. 250, 107122. http://dx.doi.org/10.1016/j.ecss.2020.107122.

Ruiz, J., Echevarría, F., Font, J., Ruiz, S., García, E., Blanco, J.M., Jiménez-Gómez, F., Prieto, L., González-Alaminos, A., García, C.M., Cipollini, P., Snaith, H., Bartual, A., Reul, A., Rodríguez, V., 2001. Surface distribution of chlorophyll, particles and gelbstoff in the Atlantic jet of the Alborán Sea: from submesoscale to subinertial scales of variability. J. Mar. Syst. 29, 277–292.

Sala, I., 2021. Physical-Biological Interaction in the Strait of Gibraltar: The Trafalgar-Alborán Connection (Ph.D. thesis). University of Cádiz.

Sánchez, R., Relvas, P., Martinho, A., Miller, P., 2008. Physical description of an upwelling filament west of Cape St. Vincent in late 2004. J. Geophys. Res. 113, http://dx.doi.org/10.1029/2007JC004430.

Sánchez-Garrido, J.C., García-Lafuente, J., Álvarez Fanjul, E., García Sotillo, M., De los Santos, F.J., 2013. What does cause the collapse of the Western Alboran Gyre? Results of an operational ocean model. Prog. Oceanogr. 116, 142–153. http://dx.doi.org/10.1016/j.pocean.2013.07.002.

Sánchez-Garrido, J.C., Naranjo, C., Macías, D., García-Lafuente, J., Oguz, T., 2015. Modeling the impact of tidal flows on the biological productivity of the Alborán Sea. J. Geophys. Res. Oceans 120, 7237–7252. http://dx.doi.org/10.1002/2015JC010969.

Sarhan, T., García-Lafuente, J., Vargas, M., Vargas, J.M., Plaza, F., 2000. Upwelling mechanisms in the northwestern Alborán Sea. J. Mar. Syst. 23, 317–331. http://dx.doi.org/10.1016/S0924-7963(99)00068-8.

Sotillo, M.G., Amo-Baladrón, A., Padorno, E., García-Ladona, E., Orfila, A., Rodríguez-Rubio, P., Conti, D., Jiménez Madrid, J., De los Santos, F.J., Álvarez-Fanjul, E., 2016. How is the surface Atlantic water inflow through the Gibraltar Strait forecasted? A lagrangian validation of operational oceanographic services in the Alborán Sea and the Western Mediterranean. Deep-Sea Res. II 133, 100–117. http://dx.doi.org/10.1016/j.dsr2.2016.05.020.

Strickland, J., Parsons, T., 1972. A Practical Handbook of Seawater Analysis, Vol. 167, second ed. Bulletin of Fisheries Research Board of Canada, Ottawa.

Szegedy, C., Ioffe, S., Vanhoucke, V., Alemi, A., 2016. Inception-v4, Inception-ResNet and the impact of residual connections on learning. In: Thirty-First AAAI Conference on Artificial Intelligence. AAAI, San Francisco.

Vargas, J.M., García-Lafuente, J., Delgado, J., Criado-Aldeanueva, F., 2003. Seasonal and wind-induced variability of sea surface temperature patterns in the Gulf of Cádiz. J. Mar. Syst. 38, 205–219. http://dx.doi.org/10.1016/S0924-7963(02)00240-3.

Vélez-Belchí, P., Vargas-Yáñez, M., Tintoré, J., 2005. Observation of a western Alborán gyre migration event. Prog. Oceanogr. 66, 190–210. http://dx.doi.org/10.1016/j.pocean.2004.09.006.

Viúdez, Á., Tintoré, J., Haney, R.L., 1996. Circulation in the Alboran Sea as determined by quasi-synoptic hydrographic observations. Part I: Three-dimensional structure of the two anticyclonic gyres. J. Phys. Oceanogr. 26, 706–724. http://dx.doi.org/10.1175/1520-0485(1996)026<0706:CITASA>2.0.CO;2.

Wasmund, N., Siegel, H., Bohata, K., Flohr, A., Hansen, A., Mohrholz, V., 2016. Phytoplankton stimulation in frontal regions of benguela upwelling filaments by internal factors. Front. Mar. Sci. 3, 210. http://dx.doi.org/10.3389/fmars.2016.00210.

Wesson, J., Gregg, M., 1994. Mixing at camarinal sill in the strait of gibraltar. J. Geophys. Res. 99, 9847–9878. http://dx.doi.org/10.1029/94JC00256.